THE PROTO-ETA SMALL-ASPECT-RATIO EXPERIMENT

G.O. LUDWIG, Y. ASO, J.J. BARROSO,
J.L. FERREIRA, R.M.O. GALVÃO, A. MONTES,
G.M. SANDONATO, M. UEDA
Laboratório Associado de Plasma,
Instituto Nacional de Pesquisas Espaciais,
São José dos Campos

W.P. DE SA, A.G. TUSZEL
Instituto de Física,
Universidade de São Paulo,
São Paulo

L.C.S. GOES
Instituto Tecnológico de Aeronáutica,
Centro Técnico Aeroespacial,
São José dos Campos

Brazil

Abstract

Proto-ETA is a small-aspect-ratio tokamak (or "spherical torus") currently under design at the "Instituto Nacional de Pesquisas Espaciais" (National Institute for Space Research - INPE) in collaboration with the Oak Ridge National Laboratory. The main objective of the device is to characterize the properties and the performance of low-aspect-ratio tokamak plasmas at relevant current and temperatures. This paper reports the current status of the conceptual design and discusses the models used to predict the operational regime and to design the main components of the device.

I. INTRODUCTION

Small-aspect-ratio tokamaks have been proposed to enhance the value of the parameter beta from a maximum of around 5% on current standard devices to 10% or more needed for economical fusion reactors [1,2]. Here beta is defined as $\beta = 2\mu_0 \langle p \rangle / B_0^2$, where $\langle p \rangle$ is the average value of the kinetic pressure and B_0 is the value of the vacuum toroidal magnetic field at the geometric center of the cross-section of the plasma column. Recently, high values of β have been obtained in highly elongated ($k > 2$) discharges in D-IIID [3]. These discharges require careful feedback control of the shape of the cross-section and vertical position of the plasma column. Equilibrium calculations indicate that small-aspect-ratio axisymmetric configurations have substantial elongation in a straight vertical field. This "natural elongation" leads to enhanced vertical stability and the tight aspect ratio also enhances the stability to ballooning and global ideal MHD modes [4,5]. Consequently, achievement of high values of β is facilitated in these configurations. The saturated width of magnetic islands due to the quasilinear evolution of single tearing modes is also predicted to decrease with aspect ratio [6]. This can lead to enhanced energy confinement if anomalous transport is indeed related to the magnetic topology of the equilibrium configuration [7,8].

One important issue with regard to the performance of compact configurations is anomalous transport. The trapped particle population increases as the aspect ratio decreases whereas the width of their orbits is expected to decrease[9]. The net effect on drift modes and related anomalous transport remains to be thoroughly investigated. Neoclassical effects upon the parallel plasma resistivity and bootstrap current, among others, are also expected to be greatly enhanced in small-aspect-ratio tokamaks. Thus, the experimental and theoretical investigation of the performance of spherical tori can substantially broaden the knowledge of the physics of tokamaks and have influence on the design of fusion reactors. In particular, current scaling laws for the energy confinement time in tokamaks are based upon data with insufficient discrimination of geometry related parameters[10]. The shape-size index $f_s = 0.32A(ak^2)^{1/4}$, where $A = R_0/a$ is the aspect ratio, R_0 and a are the major radius and halfwidth of the plasma column, and k is the elongation of the plasma cross-section, is approximately 1.0 ± 0.1 in almost all devices currently in operation. This factor can be substantially reduced in spherical tori offering the possibility to extend the database for scaling laws in the least varied direction of the parameter space[10].

The main objective of the Proto-ETA project is to design and construct an inexpensive device to investigate the performance of small-aspect-ratio axisymmetric configurations and study relevant physical processes such as stability and transport. A schematic drawing of the device is shown in Fig. 1 and the main parameters are
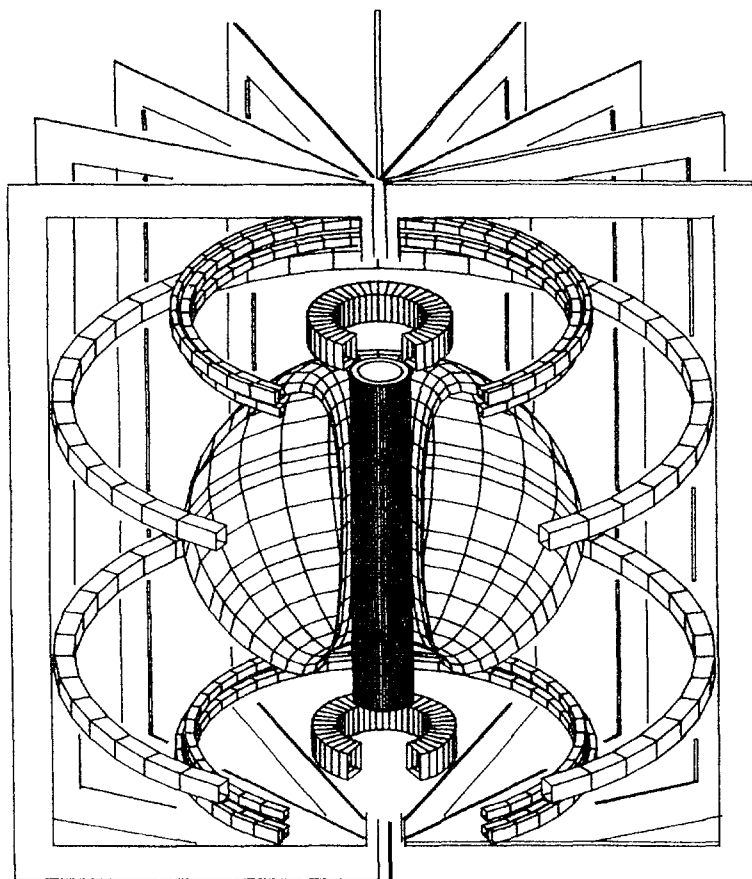
FIG. 1. Schematic diagram of Proto-ETA.

160

listed in Table I. The crucial component in the design of a spherical torus is the main induction solenoid due to the small space available between the vacuum chamber and the center post of the toroidal field coils. Furthermore, currents induced in the center post can reduce the flux available to drive the plasma current. The design of the induction solenoid of Proto-ETA follows the concept developed in Oak Ridge for the solenoid of STX[9]. A detailed analysis of the conceptual design is presented in the sequel. A maximum plasma current $I_p = 240\,\text{kA}$ can be induced in the plasma for at least 100 ms. Thus, the values of characteristic plasma quantities and dimensionless parameters to be obtained in Proto-ETA discharges are expected to be relevant for comparison with discharges in standard tokamaks[11].

TABLE I.   Major parameters of Proto-ETA conceptual design

design values	
major radius	$R_0 = 0.36\,\text{m}$
half-width of plasma column	$a = 0.24\,\text{m}$
aspect ratio	$A = 1.5$
elongation	$k = 1.8$
triangularity	$\delta = 0.35$
toroidal magnetic field (vacuum)	$B_0 = 0.36\,\text{T}$
plasma current	$I_p = 0.24\,\text{MA}$
cylindrical safety factor $\left[2\pi a^2 B_0 \left(\frac{1+k^2}{2}\right)/(\mu_0 R_0 I_p)\right]$	$q_c = 2.5$
expected values	
maximum average density (Hugill-Murakami)	$n = 10^{20}\,\text{m}^{-3}$
density averaged temperature(for 1.5 V loop voltage)	$T = 390\,\text{eV}$
average poloidal beta (Shafranov)	$\beta_I = 0.35$
maximum total β (MHD limit)	$\beta = 0.12$
effective charge number	$Z_{eff} = 1.5 \sim 2.5$

II. PLASMA PERFORMANCE

One of the physics issues of major relevance for Proto-ETA is plasma performance, i.e., energy confinement, stability and operational limits. Full inductive operation is predicted for the experiment in its basic role; auxiliary heating and current drive will be considered in a extended phase of the research program.

Recent experimental results indicate that, at least for large tokamaks, the density limit is an edge density limit. For insufficient heating power, densities at the plasma edge above a critical value lead to rapid cooling and equilibrium collapse. Empirical scalings, such as the Hugill-Murakami, do not give the correct dependence on the parameters and the connection between central and edge densities. Even though, the maximum density achievable in Proto-ETA can be estimated using the empirical expression

$$n_{20} = \nu \frac{B_0}{R_0 q_c}, \tag{1}$$

where n_{20} is the average plasma density in units of $10^{20}\,\mathrm{m}^{-3}$, ν is a constant and $q_c = \pi a^2 B_0(1 + k^2)/(\mu_0 R_0 I_p)$ is the cylindrical safety factor. Taking $\nu \simeq 2.5$, an average density limit $n \simeq 10^{20} m^{-3}$ is obtained.

To estimate the density averaged temperature, $T = \langle n_e T_e + n_i T_i \rangle / n$, where n_e, T_e and n_i, T_i are the densities and temperatures of electrons and ions, respectively, one uses a simple model for the global power balance which is described by the equation

$$\frac{\partial Q}{\partial t} = -\frac{Q}{\tau_E} + W_Q. \tag{2}$$

In this equation $Q = 3nTV_p$ is the plasma energy content, V_p is the plasma volume, τ_E is the energy confinement time, and W_Q is the net heating power given by

$$W_Q = W_\Omega - W_R + W_A, \tag{3}$$

where W_Ω is the ohmic heating power, W_R is the radiated power due to bremsstrahlung, and W_A is the auxiliary heating power, taken equal to zero for ohmic operation. The model takes into account profile, impurity, and neoclassical effects on W_Ω and W_R but neglects the strong paramagnetism and bootstrap current expected in small-aspect-ratio configurations. The energy confinement time τ_E is calculated using different L-Mode scaling laws. Assuming the Neo-Alcator scaling[12], one obtains $\tau_E = 2.2\,\mathrm{ms}$ and a loop voltage $V_l = 4.0\,\mathrm{V}$ for $Z_{eff} = 2.0$. This value of the loop voltage is considered excessive as compared to experimental results which indicate that a value of V_l within the range $1.0 \sim 2.0\,\mathrm{V}$ should be expected[13]. Accordingly, a model was developed for ohmic operation in which the value of V_l is fixed a priori; neglecting the radiated power in steady-state one obtains

$$\tau_E \sim \frac{nR_0^2 k^{1/3} q_c^{1/3}}{V_l^{5/3} B_0^{1/3}(1 + k^2)^{1/3}}. \tag{4}$$

The plasma operation contours in the ohmic regime are shown in Fig. 2 for different values of the loop voltage. An average plasma temperature in the range $390 < T < 510\,eV$ can be expected for $1.5 > V_l > 1.0\,V$, which corresponds to $11 < \tau_E < 22\,\mathrm{ms}$. Using the standard expression for τ_E, one obtains $T = 200\,\mathrm{eV}$ and $V_l = 4.0\,\mathrm{V}$, as mentioned above. Provision is being made for additional power for auxiliary heating and current drive after the initial ohmic heating phase of Proto-ETA. With auxiliary heating, the energy confinement time is taken to scale as $\tau_E \sim W_Q^\alpha$, where $\alpha = -0.5$ for most empirical laws. The operation contours for the Kaye-big scaling law[14] are shown in Fig. 3 for ohmic equilibrium and for additional power levels $W_A = 1.0$ and $2.0\,\mathrm{MW}$.

It must be pointed out that large discrepancies result from the application of different scaling laws. The reason for these discrepancies is two-fold. For basically similar empirical scaling laws, a geometrical factor of about two results in the values predicted for the energy confinement time due to the value of the shape-size index f_s mentioned in the introduction. For scaling laws with different dependence on the plasma parameters (different physics, as Rebut-Lallia and Lackner-Gottardi, for instance), one order of magnitude discrepancy in the value of τ_E can result. Of course,
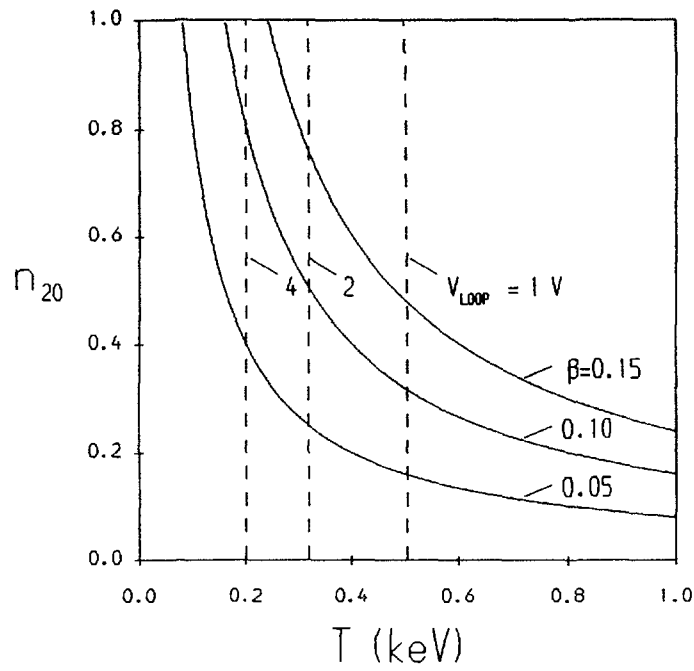
FIG. 2. Plasma operation contours for Proto-ETA in ohmic regime and for different values of the loop voltage.
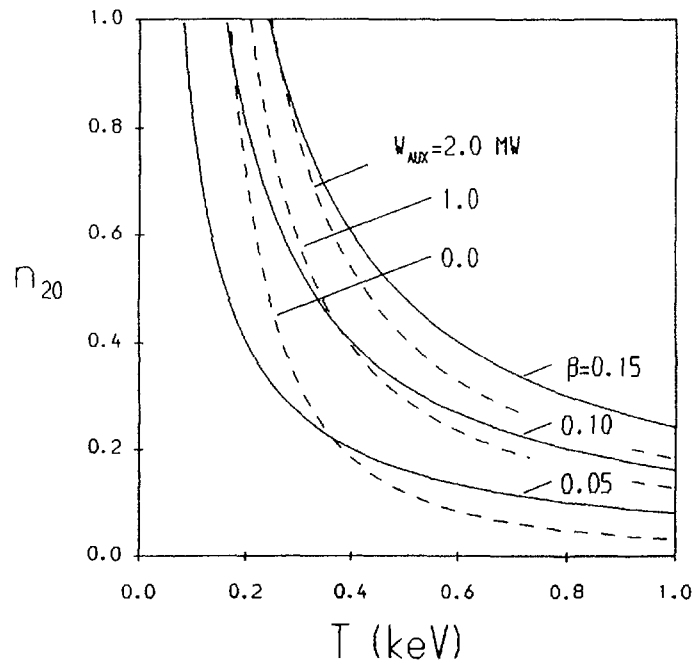
FIG. 3. Plasma operation contours for Proto-ETA with auxiliary heating assuming Kaye-big scaling[14].

one of the main objectives of a small-aspect-ratio experiment such as Proto-ETA is to help clarify the uncertainties in the scaling of τ_E.

Considering the MHD operational limits for β and for the safety factor q and assuming the Troyon-Sykes scaling, $\beta = 10^{-8}gI_p/(aB_0)$, a two-fold increase in the value of β can be immediately obtained if the aspect ratio is reduced from the standard value $R_0/a = 3.0$ to 1.5, for the same value of the cylindrical safety factor. Actually, β values over 10% are expected for stable discharges in Proto-ETA with careful control of the current-density profile. Figure 4 shows a stable equilibrium obtained for Proto-ETA using a fixed boundary equilibrium and stability code. It can be noted that the pressure profile is rather broad and the current-density profile is almost hollow, producing a very flat q profile. For this equilibrium $q_0 = 1.3$, $q_a = 4.8$ and $\epsilon\beta_I = 0.23$ giving $\beta = 0.12$ with a reasonable paramagnetic effect $(B_t/B_0 \simeq 1.2$ at the magnetic axis). Here q_0 and q_a are the values of the safety factor at the magnetic
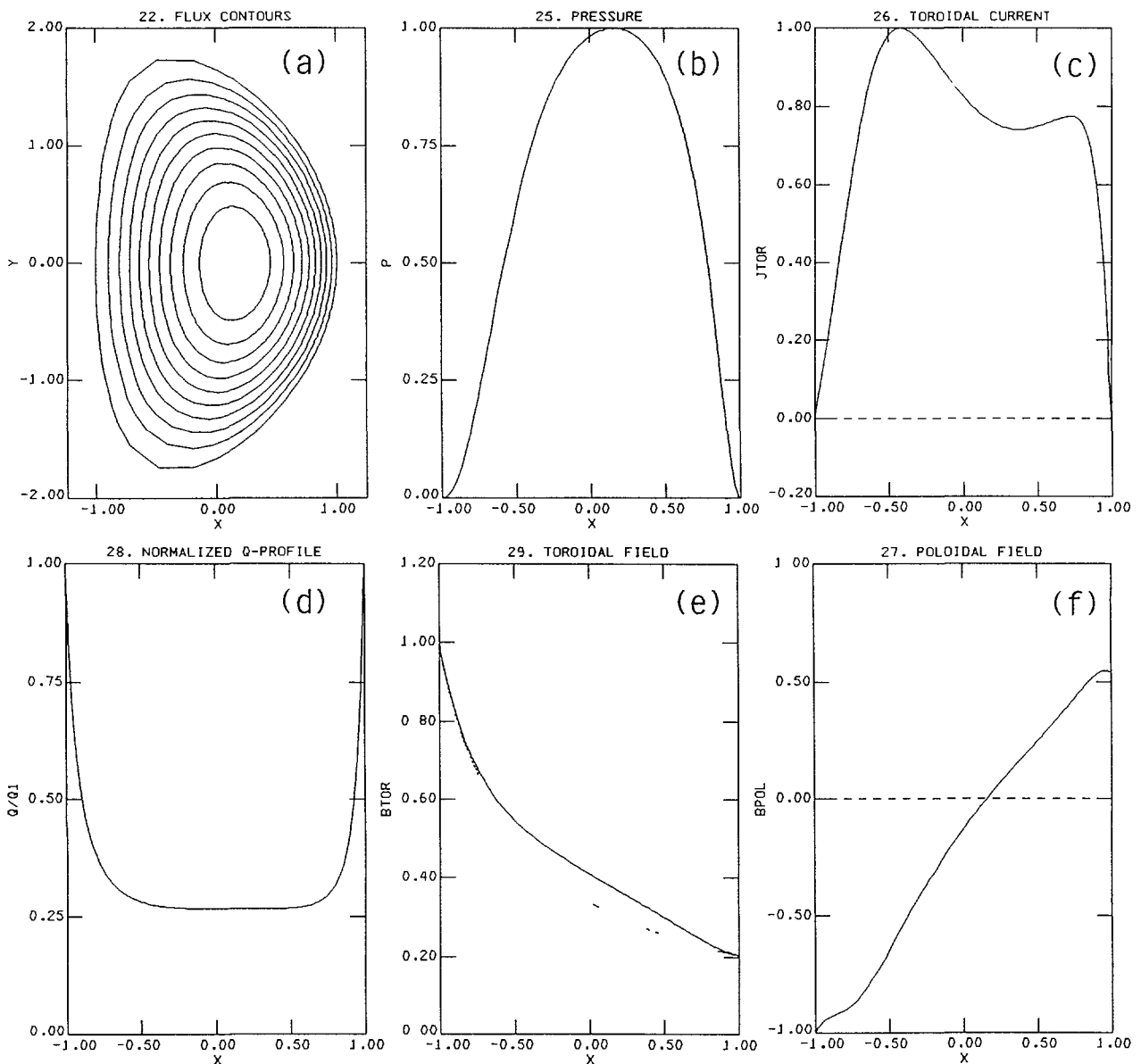
FIG. 4. Stable MHD equilibrium profiles for Proto-ETA: (a) flux surfaces; (b) pressure; (c) toroidal current density; (d) normalized q (q/q_a); (e) toroidal magnetic field; (f) poloidal magnetic field. In (e) the dashed line corresponds to the field in vacuum.

axis and at the plasma boundary, respectively, and the poloidal beta is defined as $\beta_I = 8\pi S\langle p\rangle_s/(\mu_0 I_p^2)$, where S is the area of the poloidal cross-section of the plasma column. To maintain the value of q_0 above one, non-inductive current drive or strong bootstrap current will certainly be required.

III. START-UP MODEL

A simple zero-dimensional model is used to calculate the power supply requirements for the star-up and maintenance of the full plasma current in Proto-ETA. The plasma column is modelled as a single current loop with a temperature-dependent resistance coupled to the main induction solenoid. The circuit equations are advanced in time together with the power balance equation, Eq. 2, and the particle balance equations

$$\frac{\partial n_0}{\partial t} = -n n_0 S(T) + P_0 \tag{5}$$

and

$$\frac{\partial n}{\partial t} = -\frac{n}{\tau_p} + n n_0 S(T), \tag{6}$$

where n_0 is the density of neutral particles, $S(T)$ is the ionization rate, P_0 is the particle refuelling rate, and τ_p is the particle confinement time; one takes $\tau_p \simeq 2\tau_E$. The equivalent circuit and the current waveform in the primary circuit of the induction transformer are shown in Fig. 5. The lumped circuit parameters R_Ω and L_Ω refer to the main induction solenoid and R_m and L_m to the correction coils of the primary circuit (Section IV). One of the secondary circuits, with parameters R_t and L_t, models the induced currents in the center post of the toroidal field coils which is closely coupled with the main induction solenoid, as indicated in Fig. 6. The other secondary circuit, with parameters R_p and L_p, models the plasma loop. The plasma inductance L_p is calculated using the model of Hirschman[15] for the external self-inductance valid for small-aspect-ratio plasma loops.
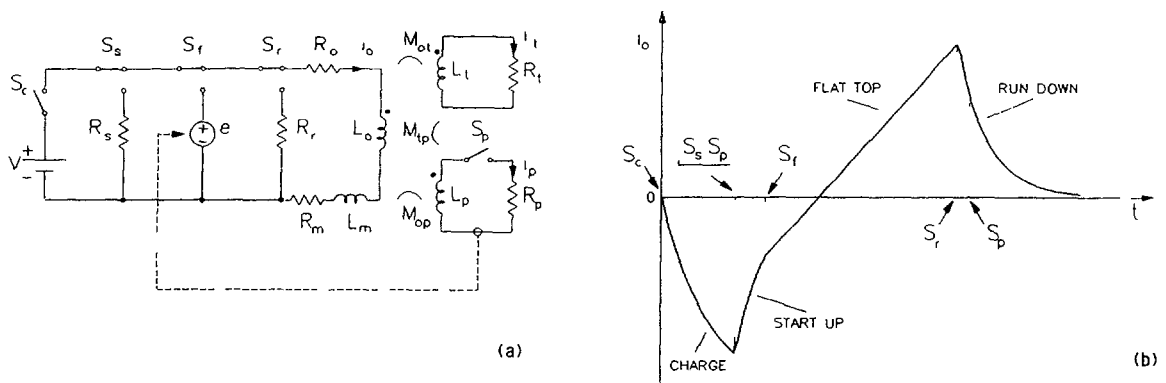
FIG. 5. Equivalent circuit (a) and schematic variation of the current in the primary circuit (b) of the induction transformer.

165
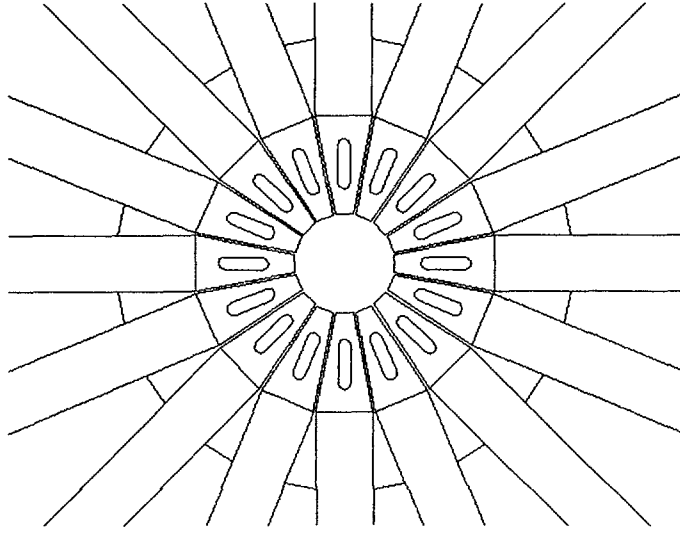
FIG. 6.   Detail of the toroidal field coils central column.

To estimate the parameters of the induction current loops in the central legs of the toroidal field coils, a simplified model is used. Each one of the N cylindrical wedged sectors and cooling holes which constitute the center post, as shown in Fig. 6, is approximated by confocal elliptic cylinders. The magnetic diffusion equation is solved in elliptic-cylinder coordinates in the low magnetic Reynolds number approximation.

This model is thus valid only if the time scale of variation of the external flux is larger than the characteristic decay time of the induced currents. The resistance and self-inductance associated with each induction current loop is calculated from the eddy current distribution. The mutual inductance of the sectors and the main induction solenoid is calculated assuming that the main solenoid links the total magnetic flux generated by the eddy currents in each sector. With this model one finds that the decay time of the induced currents is less than 2 ms for $N = 16$ coils in Proto-ETA. In Table II the values of all the parameters in the equivalent circuit of the induction transformer are given.

TABLE II.   Lumped circuit parameters of the circuit model for the induction transformer

main solenoid	$R_\Omega = 9.55\,\text{m}\Omega$ ($\sim 65\,\text{C}$)	$L_\Omega = 315\,\mu\text{H}$
magnetizing (correction) coils	$R_m = 0.678\,\text{m}\Omega$ ($\sim 35\,\text{C}$)	$L_m = 76.4\,\mu\text{H}$
induced current loops	$R_t = 4.14\,\mu\Omega$	$L_t = 5.76\,\text{nH}$
plasma loop	$R_p = 1.50/T_{keV}^{3/2}\,\mu\Omega$	$L_p = 0.229\,\mu\text{H}$
mutual inductances	$M_{\Omega p} = 2.82\,\mu\text{H}$	$M_{\Omega t} = 0.930\,\mu\text{H}$
	$M_{tp} < 7\,\text{nH}$	

166

The temporal profile of the current in the primary circuit is shown in Fig. 5(b). Initially, the induction coils are energized by switching the power supply V. At the end of the charging period, the induction coils are discharged on the load resistance R_s to provide fast flux variation for plasma breakdown (ECRH assisted) and current ramp-up. When the plasma current reaches the desired flat-top value a feedback controlled power supply e is switched on to keep the current constant against resistive decay. Finally, at the end of the flat-top period the discharge is quenched by letting the primary current decay on the load resistance R_r. The duration of the plasma current is limited by imposing a maximum temperature of 100 C or a maximum current density of 36.6 kA/cm^2 in the main solenoid, which corresponds to a peak current of 54 kA in the power supply. In Fig. 7 the temporal profiles of the primary current, plasma current, plasma temperature, neutral particle density, and plasma density are shown for a typical simulation. The particle refuelling rate P_0 is adjusted in the simulation to give a desired plasma density during flat-top. For this case, the power supply has to provide a peak power of 36 MW and an average power of ~ 10 MW.
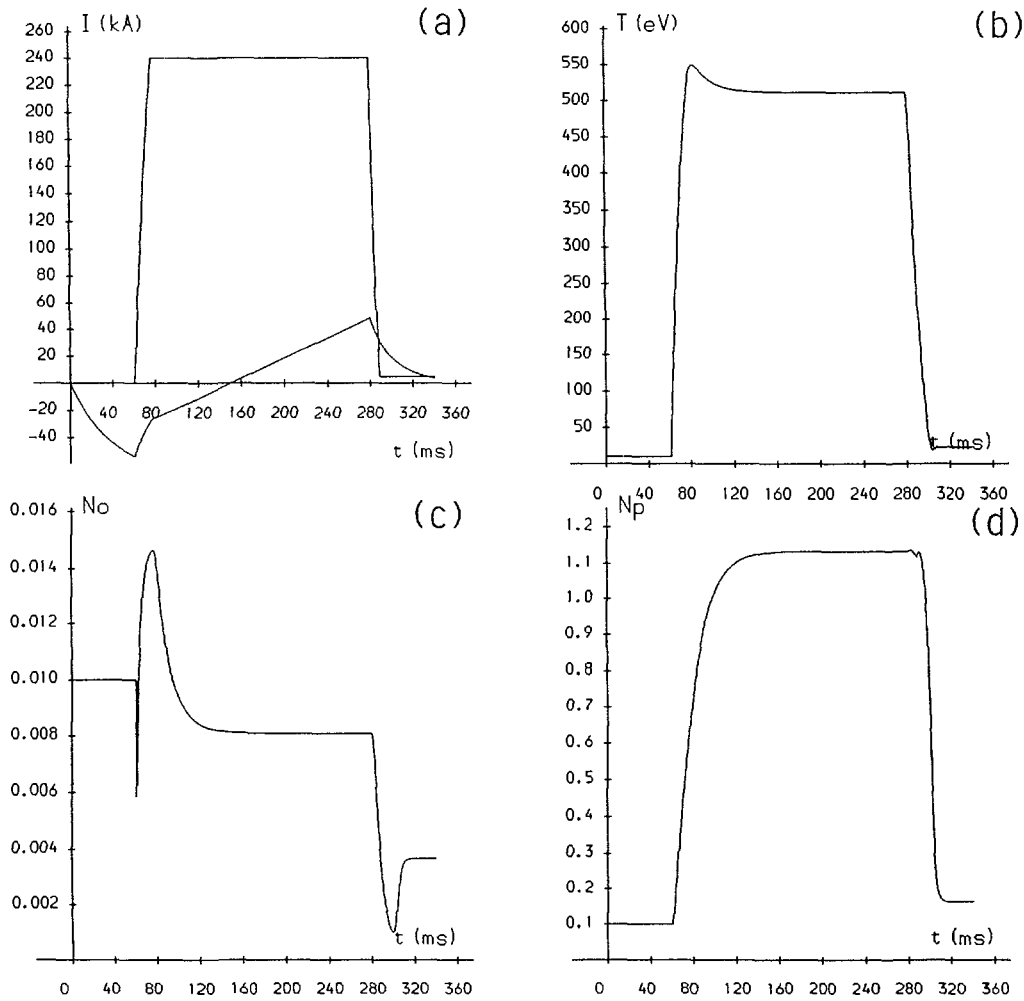
FIG. 7.   Temporal profiles of the currents in the primary circuit and in the plasma (a), the plasma temperature (b), the neutral particle density (c), and the plasma density (d) for a typical discharge in Proto-ETA. The densities are in units of 10^{19} m^{-3}.

IV. POLOIDAL COIL SYSTEM

The poloidal coil system includes the main induction solenoid, the magnetizing or correction coils to minimize the strong field in the plasma region, and the equilibrium coils. The positions of the different coils have been chosen such as to have a reasonable space between coils for diagnostic purposes.

The main solenoid will be made of GlidCop AL-15 conductor and has two layers of 66 turns each. The inner radius is 6.6 cm, the external radius is 8.8 cm, the total lenght is 1.11 m, and the packing factor is 0.78. For a maximum current density of $36.6\,kA/cm^2$, the tangential stress in the inner surface of the solenoid is 97 MPa, well below the yield strength of 310 MPa for GlidCop.

The magnetizing and the equilibrium coils will be made of OFHC copper in half hard condition with a central hole for water cooling. They are designed to carry a maximum current density of $8\,kA/cm^2$. The positions of the magnetizing coils have been chosen to yield a high null at the expected position of the magnetic axis, as shown in Fig. 8. A sixth-order null is produced with a field smaller than 1.2 mT in a region of approximately 10 cm radius around the magnetic axis. The inner coils, closer to the main solenoid, have 8 turns and the outer ones, packed together with the shapping and radial field coils, have just one turn.
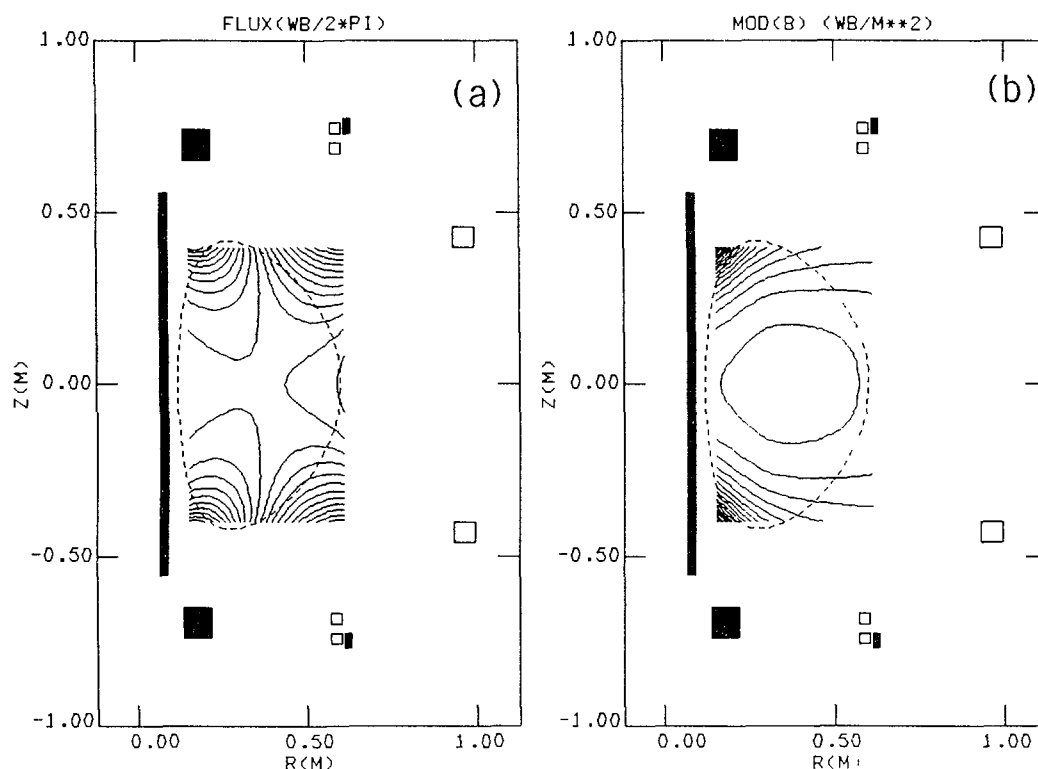
FIG. 8. Field pattern produced by the magnetizing coils (black) in Proto-ETA.

The main equilibrium field is produced by the pair of coils at $R = 0.96$ m and $Z = \pm 0.43$ m. They produce a vertical field with an almost zero decay index at the plasma region, as indicated in Fig. 9(a). A small control of elongation is provided by the shapping coils at $R = 0.585$ m and $Z = \pm 0.685$ m, as shown in Fig. 9(b). The vertical field coils have 36 turns and the shapping coils 9 turns. Control of the vertical position of the plasma column is provided by the radial field coil just above the shapping field coil.
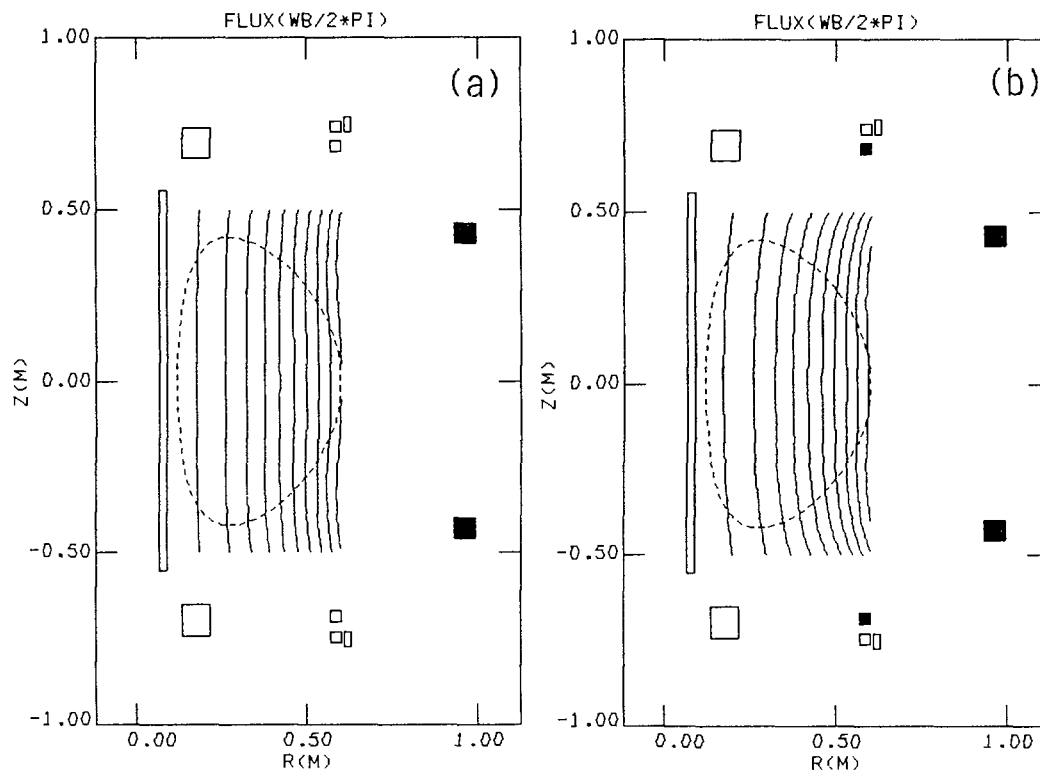
FIG. 9. Lines of force produced by the vertical field coils only (a) and vertical field plus shapping field coils (b).

V. TOROIDAL FIELD COIL

A simple design based on a picture frame geometry is adopted for the toroidal field coils, with a butt joint connecting the external legs to the central column, and lap joints connecting each of the 16 external legs to the bus bar of the power supply. The thickness of each coil is 2.24 cm and the other major dimensions are shown in Fig. 10. The inherent ripple produced with this configuration is about 0.01% at the outer edge of the plasma column ($R = 0.6$ m). Taking into account the small space available, the central column (Fig. 6) has been designed for a maximum temperature rise of 60 C during the 1.5 s effective pulse duration of the toroidal field. Cooling channels are introduced to restore the coil temperature to the initial value in a short time interval. The cooling channels have the added advantage of increasing the electrical resistance of the central column to eddy currents. The central legs are to be fabricated by extrusion of OFCH copper and bonded together as one assembly for strength and dimensional control. The power dissipated in the central column due to eddy currents
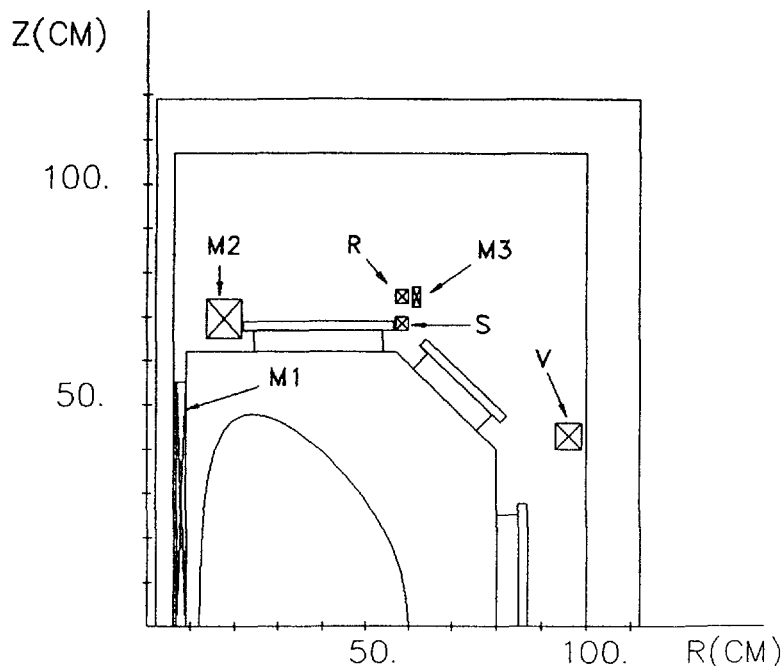
FIG. 10. Poloidal cross-section of Proto-ETA showing a toroidal field coil, and cross-sections of the vacuum chamber, the magnetizing coils M1, M2, and M3, the equilibrium coils V and S, and the radial field coil R for feedback control of the vertical position of the plasma column.

is estimated to be a small fraction of the total ohmic power. Including the cooling channels and the insulation gap between legs (1 mm), the current density at maximum field is about $8.2\,kA/cm^2$. A simple structural analysis of the coil system indicates that the coils will operate at stress levels about three times less than the maximum admissible stress for copper, even at the critical points near the external joints. The stress at the butt joint is kept at a much lower level. Presently one is considering the possibility of adopting C shaped instead of rectangular coils to minimize the bending moment along the coil, and at the butt joint in particular.

VI. POWER SUPPLIES

The power supplies needed are basically for the toroidal field coils, the induction transformer and the equilibrium field coils. The high-voltage power grid has been selected as power source for the three types of supplies. For the toroidal field supply a 12 pulses bridge rectifier using a 2.5 MVA transformer with a 90 V RMS no-load voltage is perfectly adequate. A 2.5 MVA autotransformer with adjusting taps will be introduced to cover the $B_0 = 0.1$ to $0.4\,T$ range.

The power supply for the magnetizing coils is more demanding. Two dual secondary 5 MVA transformers are needed to attain a peak power level of 45 MW and peak voltage level of 800 V. A 24 pulses transformer/rectifier system will be adopted to reach a rise time of about 3 ms for the current control loop.

170

VII. VACUUM SYSTEM

A cross-section of the vacuum chamber is shown in Fig. 10. The vessel will be continuous and thus it has to be sufficiently resistive to avoid large induced currents. The maximum allowed thickness of the inner wall is estimated from the maximum value of the loop voltage during star-up. The current flowing in the wall is given by $I = (Vh/(2\pi r\rho))\Delta r$, where h, r, Δr, and ρ are respectively the height, radius, thickness and resistivity of the wall. To estimate the maximum allowed current, the resulting error field at the geometric axis of the plasma column is imposed to be smaller than $0.1 \, mT$. Considering the wall as a short solenoid, the field produced at the geometric axis ($R_0 = 0.36 \, m$) is $B(T) = 6.7 \times 10^{-9} I(A)$, for $h = 1.32 \, m$ and $r = 0.09 \, m$. Thus the maximum allowed current is $I = 14.8 \, kA$. Assuming that the maximum loop voltage during star-up is $V \simeq 7 \, V$, one obtains $\Delta r = 0.9 \, mm$. Considering however that the stress during disruptions can be of the order of $1 \, atm$, the design value is taken to be $\Delta r = 1 \, mm$.

The vacuum chamber has large diagnostic ports which allow good access into the chamber. The large vertical ports also provide good access for neutral beam injection. The inner wall will be made from a $1 \, mm$ thick inconel tube; the other walls will be made of $5 \, mm$ thick inconel plates. Presently a modification in the design of the chamber is being considered in order to use BRIGHTON 80-10 ASME heads for the top and bottom of the chamber. These heads come in standard sizes and are made of stainless steel or inconel. Spacers will be used to provide a constant clearance between the inner wall of the vacuum chamber and the induction solenoid. Conflat seals will be used at the diagnostic ports so that baking and discharge cleanning at high wall temperatures will be possible.

Graphite limiters covered with a layer of titaniun carbide will be used covering the inner wall of the chamber. However, similar stainless stell limiters will be used for comissioning and initial operation of the device.

A total pumping speed of $4000 \, l/s$ will be made available by two turbomolecular pumps, a $500 \, m^3/h$ Roots pump, and a $80 \, m^3/h$ two-stage rotary pump.

VIII. AUXILIARY HEATING

Wave heating and current drive in Proto-ETA will probably be inefficient because lower hybrid accessibility and electron cyclotron wave absorption are made difficult by the low field and high density. Alfvén wave heating and helicity injection are interesting schemes to be investigated in small-aspect-ratio tokamaks. However, because they are not yet fully demonstrated schemes, neutral beam injection is being considered as the first alternative for auxiliary heating in the extended phase of Proto-ETA (high-beta operation). Two neutral beam injectors of $20 \, keV$ particle energy are envisaged for Proto-ETA. The beamlines are at right angles, as shown in Fig. 11. The beams can penetrate into a large portion of the plasma column without hitting the inner wall of the vacuum chamber. A simple pencil model and a Solev'ev equilibrium model were used to calculate the neutral beam shinethrough. The results are shown in Fig. 12 for a central plasma density $n(0) = 0.5 \times 10^{20} \, m^{-3}$ and for different im-
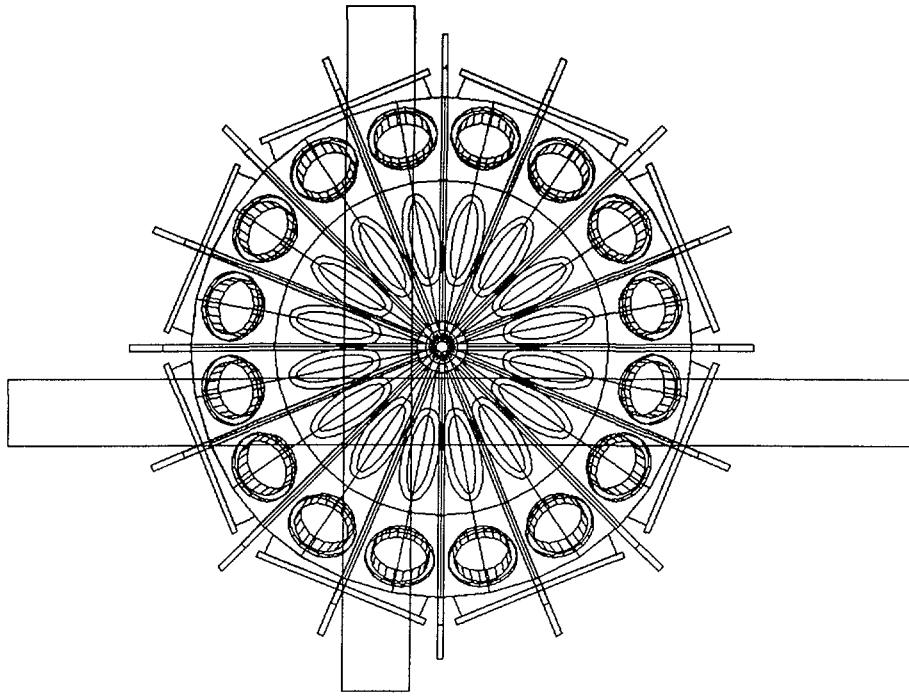
FIG. 11. Top view of Proto-ETA showing access of neutral beam injectors.

PROTO-ETA E_b = 20.0 keV

Solovev Equilibrium Model N_e = 0.50E 20m^{-3}
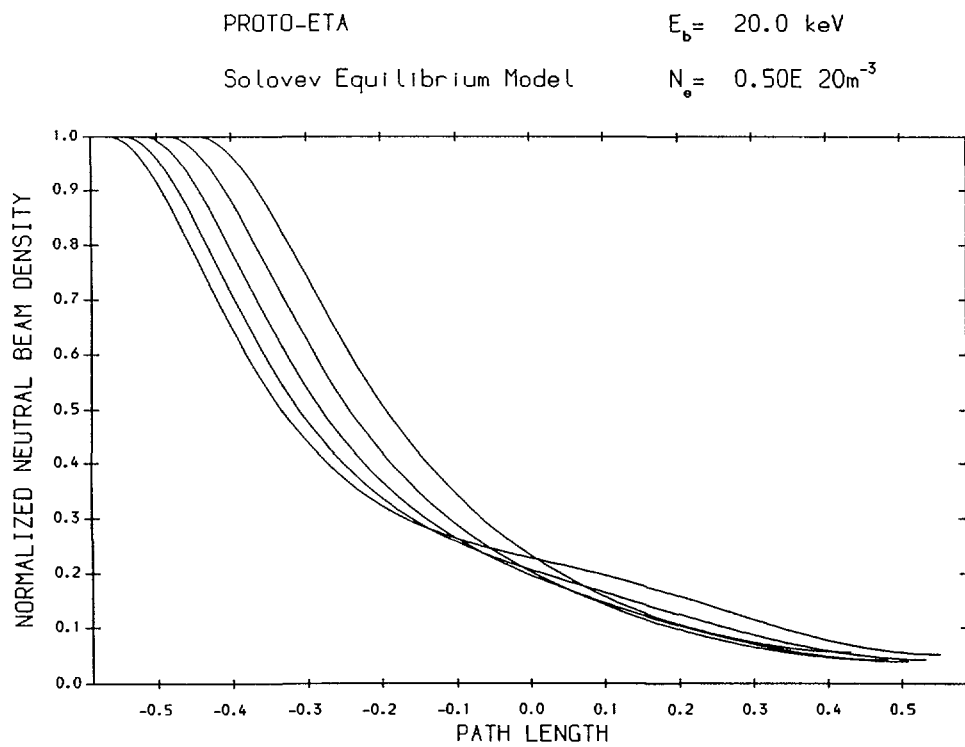
FIG. 12. Neutral beam shinethrough for a 20 keV beam, 0.5×10^{20} m^{-3} central plasma density, and different impact parameters.

pact parameters. It can be verified that for the large densities expected in high beta operation there is good beam absorption.

IX. DIAGNOSTIC SYSTEMS

The different diagnostic systems for Proto-ETA are divided in two groups: the first includes diagnostic systems that are considered essential for the ohmic operation phase of the device in which maximizing the value of β is not considered a major goal; the second is for the extended phase of operation in which auxiliary heating is envisaged. In the first group are included magnetic loops, electrostatic probes, Thomson scattering system, 2 mm microwave interferometer, spectrometer (ion temperature), thermocouples, bolometers and TV/VCR. In the second group are included upgraded magnetic loops, 1 mm microwave interferometer, heavy-ion beam probe, multi-channel Thomson scattering system, soft X-ray diodes, neutral beam probe, upgraded bolometer system, upgraded spectrometer and polarimeter.

X. CONTROL AND DATA ACQUISITON SYSTEM

The Proto-ETA Control and Data Acquisiton System (CODAS) is comprised of three main sub-systems: the plasma data acquisiton system (DAC), the machine control and monitoring system (MCMS), and the interlocking system. The CODAS primary objective is to integrate the basic functions of plasma data acquisiton and storage, machine control and sequencing of operations, and safety and security interlocking for personnel and sub-systems integrity.

The plasma data acquisiton system (DAC) is based on a micro-Vax computer interfaced with a serial highway CAMAC link. The connection between the computer and the serial highway driver is a standard asynchronous line. The CAMAC crates are controlled with standard L-2 crate controllers. The link between the crate controllers is done with optical cables through U-type adapters. A master timing generator and time delay modules provide the triggering and synchronization signals to the CAMAC crates.

The connection between the main DAC computer and the machine control and monitoring system (MCMS) is done through a PC based supervisory work station. The MCMS is a distributed control and data acquisiton system with three hierarchical levels. The basic functions of machine control and subsystems operational sequencing is done through a multi-drop network of programmable logic controllers (PLC). The dedicated PLC's (level 3) are coordinated by a master PLC which is connected to the supervisory workstation (level 2). The main DAC computer (level 1) is linked to a host computer in a Vax cluster.

XI. CONCLUSIONS

An overview of the conceptual design of Proto-ETA has been presented. Cost estimates are not yet completed but preliminary figures indicate that the basic device shall cost around five millions dollars. Thus, the device will allow relevant tokamak physics to be investigated at low aspect-ratios with a very good cost/benefit ratio. The

conceptual design has recently been reviewed by a team of physicists and engineers from INPE and Oak Ridge National Laboratory; the final report on the design will be completed by the end of this year. Preliminary arrangements are being made in Brazil between various plasma groups and financing agencies to assemble technical and financial support for the project.

REFERENCES

[1]Y-K. M. Peng, D. Strickler, Nuclear Fusion **26**, 769 (1989).

[2]Y-K. M. Peng, J. R. Haines, "The Concepts of the Compact Torus Reactor", Oak Ridge National Laboratory Report ORNL/FEDC - 88/8, Oak Ridge, TN, 1988.

[3]G. L. Taylor, T. H. Jensen, Y. Kamada *et al.*, in *Proceedings of the 13th International Conference on Plasma Physics and Controlled Nuclear Fusion Research*, Arlington, VA, October 1990 (USA), paper IAEA CN-53/A-3-1.

[4]W. Kerner, P. Gautier, K. Lakner, W. Schneider, R. Gruber, F. Troyon, Nuclear Fusion **21**, 1383 (1981).

[5]S. G. Bespoludennov, L. M. Degtyarev, S. Yu. Medvedev, Soviet Journal of Plasma Physics **12**, 441 (1986).

[6]B. A. Carreras, L. A. Charlton, J. T. Hogan, J. A. Holmes, E. A. Lazarus, W. A. Cooper, T. C. Hender, in *Proceedings of the 11th International Conference on Plasma Physics and Controlled Nuclear Fusion Research*, Kyoto, Japan, 1986 (International Atomic Energy Agency, Vienna, 1987).

[7]M. F. Turner, J. A. Wesson, Nuclear Fusion **22**, 1069 (1982).

[8]G. H. Rebut, P. P. Lallia, M. L. Watkins, in *Proceedings of the 12th International Conference on Plasma Physics and Controlled Nuclear Fusion Research*, Nice, France, 1988 (International Atomic Energy Agency, Vienna, 1989).

[9]E. A. Lazarus *et al.*, "A Feasibility Study for the Spherical Torus Experiment", Oak Ridge National Laboratory Report ORNL-TM-9786, Oak Ridge, TN, 1985.

[10]K. S. Riedel, S. M. Kaye, Nuclear Fusion **30**, 731 (1990).

[11]K. Lackner, Comments on Plasma Physics and Controlled Fusion **13**, 163 (1990).

[12]D. L. Jassby, D. R. Cohn, R. R. Parker, Nuclear Fusion **16**, 1045 (1976).

[13]R. Blanken (private communication).

[14]P. Yushmanov *et al.* (to be published in Nuclear Fusion).

[15]S. P. Hirschman, G. H. Neilson, Physics of Fluids **29**, 790 (1986).